Academic Journal of Applied Mathematical Sciences
ISSN(e): 2415-2188, ISSN(p): 2415-5225
Vol. 6, Issue. 7, pp: 100-125, 2020
URL: https://arpgweb.com/journal/journal/17
DOI: https://doi.org/10.32861/ajams.67.100.125

Academic Research Publishing Group

Original Research **Open Access**

Study of MHD Heat and Mass Transfer Flow for Hall and Ion-Slip Currents Effects in High Porosity Medium and Revolving System

Md. Delowar Hossain (Corresponding Author)
Department of Mathematics, Chittagong University of Engineering and Technology, Chittagong-4349, Bangladesh
Email: delowar_cuet@yahoo.com

Md. Abdus Samad
Department of Applied Mathematics, University of Dhaka, Dhaka-1000, Bangladesh

Md. Mahmud Alam
Mathematics Discipline, Khulna University, Khulna-9208, Bangladesh

Article History
Received: June 26, 2020
Revised: July 18,2020
Accepted: July 24, 2020
Published: July 28, 2020

Abstract

In high porosity medium and revolving system the effects of ion-slip and Hall currents are studied on MHD heat and mass transfer flow. The non-linear coupled partial differential equations are determined using byl transformations and solve these equations employing finite difference method. Velocity, temperature as well as concentration profiles are studied for the concerned physical parameters and results are presented graphically. Due to the Hall and ion-slip parameters, Eckert number, and porosity parameter the velocity profiles are pronounced while it is declined for the effects of magnetic parameter, Prandtl number. Also the magnetic parameter enhances the temperature profiles. On the other hand, the temperature (concentration) profile decreases (increases) for the increasing effect of Prandtl number (Soret number). The rate of changes of velocity, temperature and concentration profiles are also presented graphically.

Keywords: MHD; Hall and Ion-slip currents; Porosity; Rotation; Eckert number.

1. Introduction

Magnetohydrodynamics (MHD) has great deal of attention science, engineering and applied Mathematics for their importance in diverse field such as, aerodynamics, engineering, geophysics and aeronautics. Interests in MHD phenomena have existed, especially in the astrophysics community where the work of Cowling [1] and Ferraro [2] can be seen as pioneering work establishing the formal theory of MHD on an astrophysical scale.Growing interests in magnetohydrodynamics in the nineteen forties with the work of Hartmann [3].

The heat transport in a straight up surface surrounded in absorbent medium occurs in many manufacturing problems such as in heat exchangers. Free convection can observed in geophysics, astrophysics, soil sciences and so on. Natural convective flow and viscous dissipation effects are examined Gebhart [4]. Schwartz and Smith [5] have found their investigation that porosity is not stable but due to variation in permeability it varies.At fist the boundary and inertial effects on heat transfer flow is studied by Vafai and Tien [6]. Chen and Lin [7], Chamkha, *et al.* [8], Foisal and Alam [9], studied thermally stratified high porosity medium with free convection in porous medium. In high-porosity medium convective heat transfer model in thermally-stratified revolving fluid has investigated with help of finite difference method by Anwar, *et al.* [10]. MHD thermal diffusion and diffusion thermo effects on free convection unsteady flow over a moving plate have scrutinized Venkata, *et al.* [11]. Bhuvanavijaya and Mallikarjuna [12], have analyzed convective heat and mass transfer for the influence of variable thermal conductivity in a rotating system with variable porosity regime over a vertical plate. Beside, Chen, *et al.* [13] have investigated transient natural convective flow along a vertical flat plate surrounded with high-porosity media. For the effects of radiation, chemical reaction and thermal diffusion natural convective heat and mass transfer flow have studied Suneetha, *et al.* [14] in highly porous medium. MHD natural convective flow and mass transfer in incompressible unsteady viscous dissipative fluid along with vertical permeable plate have studied Reddy [15]. Dash, *et al.* [16], have explored the ion-slip and Hall currents effects on MHD convective flow and mass transfer over a vertical plate. Naroua [17], has examined MHD natural convective flow for the influence of Hall and ion-slip currents due to the rotating heat generating fluid. Along a vertical absorbent plate the thermal radiation and magnetic field effects have been studied [18] due to Hall current. Rotating parameter and Hall current effects reported Abuga, *et al.* [19] on dissipative fluid flow along vertical plate. Beside, Seth, *et al.* [20] have studied the Hall current effect within a rotating vertical channel in heat absorbing fluid. Hall and ion- slip currents effects on heat transfer flow have analyzed [21] along erect plate with slip condition. In contrast [22] analyzed the thermal diffusion, Joule heating and Hall current effects on MHD revolving free and force convective flow along vertical permeable plate. Hall Effect and influence of ion slip current above exponential accelerated plate have investigated [23] on unsteady free convective rotating flow through a saturated permeable media consequence of magnetic field. Hall current and rotation as well as Soret

effects have studied [24] on heat and mass transfer flow consequence magnetic field. Over a vertical exponential accelerated plate the Hall and ion-slip current effects have examined by Jitendra and Srinivasa [25] on convective flow with rotating fluid for magnetic field. The effects of suction, Soret and Dufour number on boundary layer flow along a revolving vertical permeable plate have studied by Srinivasa, *et al.* [26] in case of the effect of magnetic field. And found that in presence of Hall current the Coriolis as well as hydromagnetic forces contribute potential role in the characteristic flow behavior. MHD convective flow throughout a porous media in an upright exponentially accelerated flat plate for variable temperature and rotating system has reported Rajput and Mohammad [27] with Hall current. The effects of chemical reaction, Soret and Dufour number on heat and mass transfer have explored EL-Kabeir, *et al.* [28] in different flow conditions of fluid and embedded environment. MHD force convection in a rotating system has investigated [29] with Hall effect for dissipative heat in infinite porous plate. MHD heat and mass flow though a absorbent medium along a accelerated erect plate in presence of Hall current, rotation, and Soret effects have examined by Chandra [30]. Beside, [31] have studied conjugately the heat and mass transfer throughout a permeable medium in a system of rotation for the effects of viscous dissipation as well as Joule heating. The heat and mass transfer have studied [32] in porous medium over stirring vertical plate due to the effect of magnetic field with suction and viscous dissipation. The viscous dissipation effect has studied [33] on MHD convective flow along a straight up plate rotated in permeable media.

Consequence of Hall and ion-slip currents in presence of magnetic field the heat and mass transfer flow have examined considering rotational high porous medium. Using finite difference method dimensionless partial differential equations are solved. The influence of concerned physical parameters on velocity, temperature, and concentration profiles as well as rate of changes of velocity (shear stresses), temperature (Nusselt number), and concentration (Sherwood number) are investigated and presented graphically.

2. Mathematical Analysis

An unsteady Hall and ion-slip currents effects on heat and mass transfer flow in a revolving system with high porosity medium in presence of magnetic field is considered.

Figure-1. Physical configuration and coordinate system

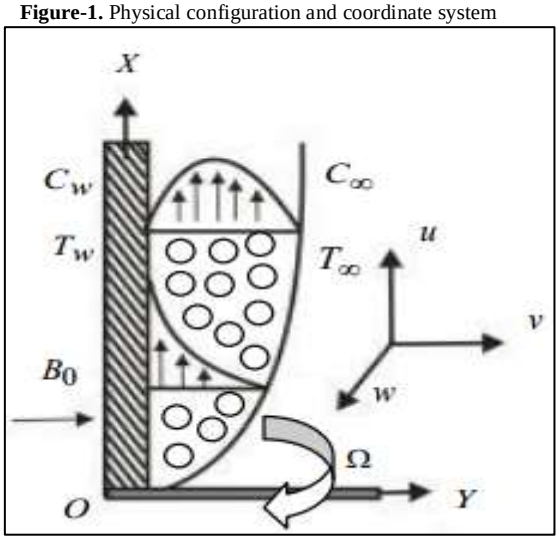

The flow is upward direction along the vertical plate which is considered the x-axis and y-axis is perpendicular to the flow. The system is rotated with constant angular velocity about y-axis. The temperature of the plat and concentration are increased to $T_w(>T_\infty)$ and $C_w(>C_\infty)$ respectively, where T_w, C_w are temperature and concentration at the wall and T_∞, C_∞ are the free stream temperature and the concentration outside the boundary layer. The geometrical configuration is presented by Figure 1. A powerful magnetic field is applied in y-direction. The magnetic field strength B_0 can be considered as $\mathbf{B}=(0,B_0,0)$. In presence of magnetic fields, Hall and ion-slip current will significantly affected for such a fluid. Magnetic Reynolds number of a partially-ionized fluid is very small, so the induced magnetic field is neglected. The equation of conservation of electric charge $\overline{\nabla}\bullet\mathbf{J}=0$ gives $J_y=$ constant because the direction of circulation is considered only along y-axis and $\mathbf{J}$ does not have any variation along the y-axis. For electrically non-conducting plate, this constant is zero i.e. $J_y=0$ at the plate and everywhere. The governing equations the flow under the above consideration and Boussinesq's approximation is given below:

The continuity equation:
$$\frac{\partial u}{\partial x}+\frac{\partial v}{\partial y}=0 \tag{1}$$

The momentum equations:

$$\frac{1}{\varepsilon^2}\left(\frac{\partial u}{\partial t}+u\frac{\partial u}{\partial x}+v\frac{\partial u}{\partial y}\right)=\frac{\upsilon}{\varepsilon}\frac{\partial^2 u}{\partial y^2}+g\beta(T-T_\infty)+g\beta^*(C-C_\infty)+2\Omega w-\frac{\upsilon}{k'}u-cu^2-\frac{\sigma B_0^2(\alpha_e u+\beta_e w)}{\rho(\alpha_e^2+\beta_e^2)} \tag{2}$$

$$\frac{1}{\varepsilon^2}\left(\frac{\partial w}{\partial t}+u\frac{\partial w}{\partial x}+v\frac{\partial w}{\partial y}\right)=\frac{\upsilon}{\varepsilon}\frac{\partial^2 w}{\partial y^2}-2\Omega u-\frac{\upsilon}{k'}w-cw^2+\frac{\sigma B_0^2(\beta_e u-\alpha_e w)}{\rho(\alpha_e^2+\beta_e^2)} \tag{3}$$

The energy equation:

$$\frac{\partial T}{\partial t}+u\frac{\partial T}{\partial x}+v\frac{\partial T}{\partial y}=\frac{\kappa}{\rho c_p}\frac{\partial^2 T}{\partial y^2}+\frac{\upsilon}{c_p}\left[\left(\frac{\partial u}{\partial y}\right)^2+\left(\frac{\partial w}{\partial y}\right)^2\right]+\frac{\sigma B_0^2(u^2+w^2)}{\rho c_p(\alpha_e^2+\beta_e^2)} \tag{4}$$

The concentration equation:

$$\frac{\partial C}{\partial t}+u\frac{\partial C}{\partial x}+v\frac{\partial C}{\partial y}=D_m\frac{\partial^2 C}{\partial y^2}+\frac{D_m k_T}{T_m}\frac{\partial^2 T}{\partial y^2} \tag{5}$$

The boundary conditions for the problems are:

$$t\le 0,\ u=0, v=0, w=0, T=T_\infty, C=C_\infty$$
$$t>0,\ u=0, v=0, w=0, T=T_\infty, C=C_\infty \text{ at } x=0$$
$$u=U_0,\ v=0,\ w=0,\ T=T_w,\ C=C_w \text{ at } y=0$$
$$u=0,\ v=0,\ w=0,\ T=T_\infty,\ C=C_\infty \text{ at } y\to\infty \tag{6}$$

where U_0 is the uniform velocity, $\alpha=1+\beta_e\beta_i$, β_e is the Hall parameter, β_i is the ion-slip parameter, y is Cartesian co-ordinate, u, v and w are the components of flow velocity in x, y and z-directions, g is the acceleration due to gravity, T_w, T_∞ are the wall temperature and free stream temperature, C_w, C_∞ are the fluid concentration and free stream fluid concentration, β is the coefficient of volumetric thermal expansion, β^* is the volumetric coefficient of expansion with concentration, Ω is the angular velocity, ρ is the density of the fluid, υ is the viscosity, k' is the magnetic permeability of the porous medium, B_0 is the uniform magnetic field of strength, D_m is the mass diffusivity, k_T is the thermal diffusion ratio, T_m is the mean fluid temperature, σ_e is the electrical conductivity of the fluid, κ is the thermal conductivity, c_p is the specific heat at constant pressure, c is the Forcheimmer (inertial) coefficient, ε is the porosity of porous medium, T is the temperature of the fluid, C is the fluid concentration.

The non-dimensional variables are given below which are used in the above equations (1)–(5),

$$X=\frac{xU_0}{\upsilon}, Y=\frac{yU_0}{\upsilon}, U=\frac{u}{U_0}, V=\frac{v}{U_0}, W=\frac{w}{U_0}, \tau=\frac{tU_0^2}{\upsilon}, \overline{T}=\frac{T-T_\infty}{T_w-T_\infty}, \overline{C}=\frac{C-C_\infty}{C_w-C_\infty} \tag{7}$$

Equations (1) –(5) becomes,

$$\frac{\partial U}{\partial X}+\frac{\partial V}{\partial Y}=0 \tag{8}$$

$$\frac{\partial U}{\partial \tau}+U\frac{\partial U}{\partial X}+V\frac{\partial U}{\partial Y}=\varepsilon\frac{\partial^2 U}{\partial Y^2}+\varepsilon^2 G_r\overline{T}+\varepsilon^2 G_m\overline{C}+2\varepsilon^2 RW-\varepsilon^2\gamma U-\varepsilon^2\Gamma U^2-\frac{\varepsilon^2 M(\alpha_e U+\beta_e W)}{\alpha_e^2+\beta_e^2} \tag{9}$$

$$\frac{\partial W}{\partial \tau}+U\frac{\partial W}{\partial X}+V\frac{\partial W}{\partial Y}=\varepsilon\frac{\partial^2 W}{\partial Y^2}-2\varepsilon^2 RU-\varepsilon^2\gamma W-\varepsilon^2\Gamma W^2+\frac{\varepsilon^2 M(\beta_e U-\alpha_e W)}{\alpha_e^2+\beta_e^2} \tag{10}$$

$$\frac{\partial \overline{T}}{\partial \tau}+U\frac{\partial \overline{T}}{\partial X}+V\frac{\partial \overline{T}}{\partial Y}=\frac{1}{P_r}\frac{\partial^2 \overline{T}}{\partial Y^2}+E_c\left[\left(\frac{\partial U}{\partial Y}\right)^2+\left(\frac{\partial W}{\partial Y}\right)^2\right]+\frac{ME_c(U^2+W^2)}{\alpha_e^2+\beta_e^2} \tag{11}$$

$$\frac{\partial \overline{C}}{\partial \tau}+U\frac{\partial \overline{C}}{\partial X}+V\frac{\partial \overline{C}}{\partial Y}=\frac{1}{S_c}\frac{\partial^2 \overline{C}}{\partial Y^2}+S_0\frac{\partial^2 \overline{T}}{\partial Y^2} \tag{12}$$

where $G_r=\frac{g\beta(T_w-T_\infty)\upsilon}{U_0^3}$ (Grashof Number), $G_m=\frac{g\beta^*(C_w-C_\infty)\upsilon}{U_0^3}$ (Modified Grashof Number), $M=\frac{\sigma B_0^2\upsilon}{\rho U_0^2}$ (Magnetic Parameter), $P_r=\frac{\rho c_p\upsilon}{\kappa}$ (Prandtl Number), $S_c=\frac{\upsilon}{D_m}$ (Schmidt Number),

$S_0 = \frac{D_m k_T (T_w - T_\infty)}{\upsilon T_m (C_w - C_\infty)}$ (Soret Number), $R = \frac{\upsilon \Omega}{U_0^2}$ (Rotational Parameter), $\Gamma = \frac{c\upsilon}{U_0}$ (Inertia coefficient), $\gamma = \frac{\upsilon^2}{k' U_0^2}$ (Permeability parameter), $E_c = \frac{U_0^2}{c_p (T_w - T_\infty)}$ (Eckert number).

The corresponding boundary conditions are:

$$\begin{gathered} \tau \le 0,\ U = 0, V = 0, W = 0, \bar{T} 0, \bar{C} = 0 \\ \tau > 0,\ U = 0, V = 0, W = 0, \bar{T} = 0,\ \bar{C} = 0 \ \text{ at } X = 0 \\ U = 1, V = 0, W = 0, \bar{T} = 1, \bar{C} = 1 \ \text{ at } Y = 0 \\ U = 0, V = 0, W = 0, \bar{T} = 0, \bar{C} = 0 \ \text{ as } Y \to \infty \end{gathered} \tag{13}$$

3. Numerical Technique

The dimensionless second order non-linear coupled partial differential equations are solved numerically by using finite difference method. In this case the region within the boundary layer is divided into grid or meshes of lines parallel to X - and Y - axes where X -axis is taken along the plate and Y - axis is perpendicular to the plate which is shown in Figure 2.

Figure-2. Finite difference grid

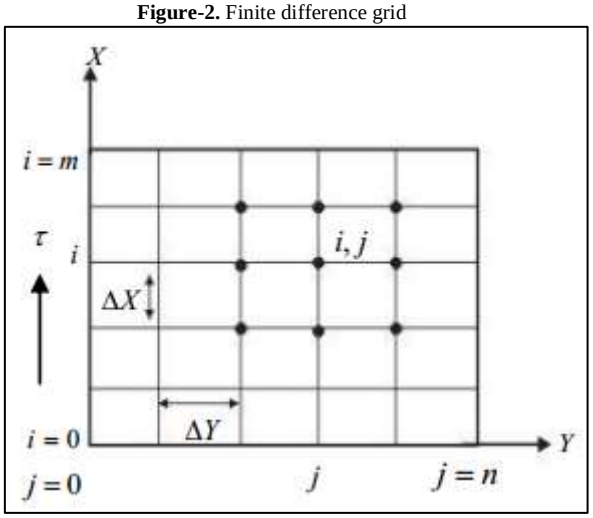

The height of the plate is considered $X_{\max}(=80.0)$ i.e. X varies from 0 to 80 and assumed $Y_{\max}(=60)$ as corresponding $Y \to \infty$ i.e. Y varies from 0 to 60. There are $m(=300)$ and $n(=300)$ grid space in the X and Y axes are shown in Figure 1, hence the constant mesh size along X and Y axes become $\Delta X = 0.27(0 \le X \le 80.0)$ and $\Delta Y = 0.2(0 \le Y \le 60)$ with the minor time step $\Delta\tau = 0.005$.

Let the values of $U, V, W, \bar{T}$ and $\bar{C}$ at the end of a time-step are denoted by $U', V', W', \bar{T}'$ and $\bar{C}'$.

The finite difference equations are obtained by from equations (8)-(12) wich are as follows:

$$\frac{U'_{i,j} - U'_{i-1,j}}{\Delta X} + \frac{V_{i,j} - V_{i,j-1}}{\Delta Y} = 0 \tag{14}$$

$$\frac{U'_{i,j} - U_{i,j}}{\Delta\tau} + U_{i,j}\frac{U_{i,j} - U_{i-1,j}}{\Delta X} + V_{i,j}\frac{U_{i,j+1} - U_{i,j}}{\Delta Y} = \varepsilon\frac{U_{i,j+1} - 2U_{i,j} + U_{i,j-1}}{(\Delta Y)^2} + \varepsilon^2 G_r \bar{T}_{i,j} + \varepsilon^2 G_m \bar{C}_{i,j} + 2\varepsilon^2 R W_{i,j} - \varepsilon^2\gamma U_{i,j} - \varepsilon^2\Gamma U_{i,j}^2 - \frac{M\varepsilon^2(\alpha_e U_{i,j} + \beta_e W_{i,j})}{\alpha_e^2 + \beta_e^2} \tag{15}$$

$$\frac{W'_{i,j} - W_{i,j}}{\Delta\tau} + U_{i,j}\frac{W_{i,j} - W_{i-1,j}}{\Delta X} + V_{i,j}\frac{W_{i,j+1} - W_{i,j}}{\Delta Y} = \varepsilon\frac{W_{i,j+1} - 2W_{i,j} + W_{i,j-1}}{(\Delta Y)^2} - 2\varepsilon^2 R U_{i,j} - \varepsilon^2\gamma W_{i,j} - \varepsilon^2\Gamma W_{i,j}^2 + \frac{M\varepsilon^2(\beta_e U_{i,j} - \alpha_e W_{i,j})}{\alpha_e^2 + \beta_e^2} \tag{16}$$

$$\frac{\overline{T}'_{i,j}-\overline{T}_{i,j}}{\Delta\tau}+U_{i,j}\frac{\overline{T}_{i,j}-\overline{T}_{i-1,j}}{\Delta X}+V_{i,j}\frac{\overline{T}_{i,j+1}-\overline{T}_{i,j}}{\Delta Y}=\frac{1}{P_r}\frac{\overline{T}_{i,j+1}-2\overline{T}_{i,j}+\overline{T}_{i,j-1}}{(\Delta Y)^2}+E_c\left[\left(\frac{U_{i,j+1}-U_{i,j}}{\Delta Y}\right)^2+\left(\frac{W_{i,j+1}-W_{i,j}}{\Delta Y}\right)^2\right]+\frac{ME_c\left(U_{i,j}^2+W_{i,j}^2\right)}{\alpha_e^2+\beta_e^2} \tag{17}$$

$$\frac{\overline{C}'_{i,j}-\overline{C}_{i,j}}{\Delta\tau}+U_{i,j}\frac{\overline{C}_{i,j}-\overline{C}_{i-1,j}}{\Delta X}+V_{i,j}\frac{\overline{C}_{i,j+1}-\overline{C}_{i,j}}{\Delta Y}=\frac{1}{S_c}\frac{\overline{C}_{i,j+1}-2\overline{C}_{i,j}+\overline{C}_{i,j-1}}{(\Delta Y)^2}+S_0\frac{\overline{T}_{i,j+1}-2\overline{T}_{i,j}+\overline{T}_{i,j-1}}{(\Delta Y)^2} \tag{18}$$

The boundary conditions are obtained as follows:

$$\begin{aligned}&U_{i,j}^0, V_{i,j}^0, W_{i,j}^0, \overline{T}_{i,j}^0, \overline{C}_{i,j}^0 = 0\\ &U_{0,j}^n, V_{0,j}^n, W_{0,j}^n, \overline{T}_{0,j}^n, \overline{C}_{0,j}^n = 0\\ &U_{i,0}^n, V_{i,0}^n, W_{i,0}^n, \overline{T}_{i,0}^n, \overline{C}_{i,0}^n = 0\\ &U_{i,L}^n, V_{i,L}^n, W_{i,L}^n, \overline{T}_{i,L}^n, \overline{C}_{i,L}^n = 0 \quad where \quad L\to\infty\end{aligned} \tag{19}$$

Here the subscripts i denote the grid points with X-axis and j denote the grid points with Y-axis and superscript n denote the value of time, $\tau = n\Delta\tau$ where $n = 0,1,2,3,....$.

The mathematical values of the local shear stress, Nusselt number and Sherwood number are calculated by five-point approximate formula for the derivatives and the average shear stress, Nusselt number and Sherwood number are calculated by Simpson's $\frac{1}{3}$ integration formula.

4. Stability and Convergence

For the constant mesh sizes the stability criteria of the scheme has been established.

$$\frac{U\Delta\tau}{\Delta X}+\frac{|-V|\Delta\tau}{\Delta Y}+\frac{2\varepsilon\Delta\tau}{P_r(\Delta Y)^2}\le 1,$$

$$\frac{U\Delta\tau}{\Delta X}+\frac{|-V|\Delta\tau}{\Delta Y}+\frac{2\varepsilon\Delta\tau}{S_c(\Delta Y)^2}\le 1$$

When $\Delta\tau$ and ΔY approach to zero then the problem will be converged. Hence the convergence criteria of the problem are $P_r \ge 0.5$, $S_c \ge 0.5$.

4.1. Shear Stress Nusselt Number and Sherwood Number

The rate of change of velocity (local shear stress) at the plate in x and z-axes are as $\tau_{LU} = \mu\left(\frac{\partial u}{\partial y}\right)_{y=0}$ and $\tau_{LW} = \mu\left(\frac{\partial w}{\partial y}\right)_{y=0}$ which are proportional to $\left(\frac{\partial U}{\partial Y}\right)_{Y=0}$ and $\left(\frac{\partial W}{\partial Y}\right)_{Y=0}$.

The following equations define the x and z components of the average shear stress are as

$\tau_{AU} = \mu\int\left(\frac{\partial u}{\partial y}\right)_{y=0} dx$ and $\tau_{AU} = \mu\int\left(\frac{\partial w}{\partial y}\right)_{y=0} dx$ which are proportional to $\int_0^{80}\left(\frac{\partial U}{\partial Y}\right)_{Y=0} dX$ and $\int_0^{80}\left(\frac{\partial W}{\partial Y}\right)_{Y=0} dX$.

5. Results and Discussion

5.1. Justification of Grid Space

To prove the effects of grid space for m and n the code is conversed with different grid space, such as $m, n = 250, 300, 400$. From Figure 3, it is seen that there is a minor change between them. According to this situation, the results of velocity, temperature and concentration have been carried out for $m, n = 300$.

5.2. Steady State Solution

The non-linear partial differential equations (9)-(12) under the boundary conditions have been solved along with explicit finite difference method. In order to verify the effects of time step size $\Delta\tau$, the programming code is conversed our model with different step sizes such as $\tau = 20, 60, 70, 80, 90, 100, 110, 120$.

Figure-3. Primary velocity for different grid space of rotational parameter R

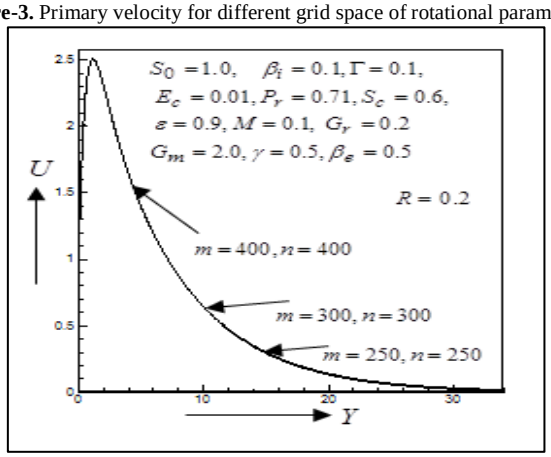

Figure-4. Primary velocity for different time step of rotation parameter R

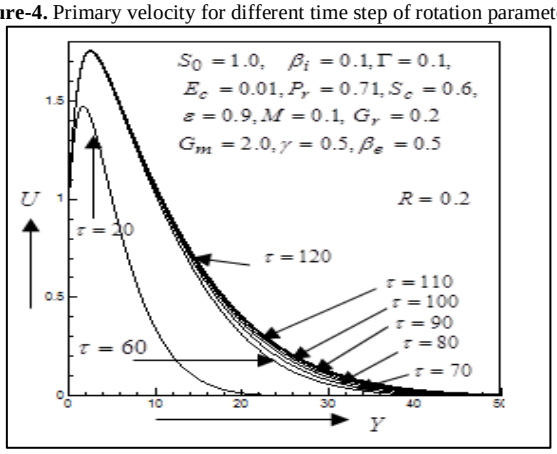

For computation of each of $U, W, \overline{T}$ and $\overline{C}$ one can consider $\tau = 100$ and found negligible change in each case after $\tau = 100$. Thus the solutions of all variables for $\tau = 100$ are said to be steady-state solution. Hence the velocity profiles, temperature and concentration profiles are drawn taking $\tau = 100$ which is displayed in Figure 4.

The dimensionless primary velocity (U), secondary velocity(W), temperature($\overline{T}$), species concentration ($\overline{C}$), local and average shear stresses in x-axis (τ_{LU}, τ_{AU}), local and average shear stresses in z-axis (τ_{LW}, τ_{AW}), local and average Nusselt numbers (N_{uL}, N_{uA}), local and average Sherwood numbers (S_{hL}, S_{hA}) are investigated for various values of the material parameters such as Hall parameter(β_e), ion-slip parameter(β_i), magnetic parameter(M), rotation parameter (R), Prandtl number(P_r), Schmidt number (S_c), Soret number(S_0), permeability parameter(γ), Eckert number (E_c), porosity parameter (ε), iteration parameter (Γ). In most cases the parameters are considered arbitrary constant. In this case $P_r = 0.71$ corresponds to air, $P_r = 1.0$ corresponds to electrolyte solution such as salt water and $P_r = 1.63$ corresponds to glycerin at $50^0 C$ and Schmidt number (S_c) the values $0.60, 1.0, 2.62$ are considered, which represent specific condition of flow (0.60 corresponds to water vapor, 1.0 correspond to carbonsioxid that represents the most common effect in air, 2.62 corresponds to propyl-benzene at $20^0 C$). G_r and G_m are taken positive. The importance of G_r and G_m are taken large such as $G_r = 5.0$ and $G_m = 2.0$.

Figures 5 (a, b, c) and Figures 7 (a, b, c), illustrate that the primary velocity, Local and average shear stress in x-axis (τ_{LU}, τ_{AU}) enhance with the increase of Hall and ion- slip parameter (β_e and β_i). This is because that the effective conductivity decreases, which reduces the magnetic resistive force affecting on the primary flow. The temperature distributions decreased when the Hall parameter increased which is illustrated in Figure 6 (a). It is clear that when Hall parameter is increased then thermal boundary layer thickness decreases, for this reason temperature distributions decreases. While Local and average Nusselt number are increased and these are displayed in Figures 6 (b, c). Also secondary velocity (W), local and average shear stresses in z-axis (τ_{LW}, τ_{AW}) have decreasing effects for increasing values of ion-slip parameter(β_i) which is found in Figure 8 (a, b, c).

By analyzing the Figure 9(a) it is clearly noted that the primary velocity profiles firstly increases in the interval $(0 \le Y \le 21.0)$ and the minor decreasing effects $Y > 21.0$ with the increasing values of Eckert number (E_c). The

Local and average shear stress in x-axis increase which are found in Figures 9 (b, c). It is seen from Figure 10 (a) temperature profiles increases with the increase of Eckert number which is shown in Figure 10 (a). The energy is increased in the boundary layer when Eckert number is increased, so temperature distributions increases.

The local and average Nusselt number has reverse effect which are illustrated in Figures 10 (b, c). Figures 11 (a, b, c) depict the effect of the porosity parameter (ε) on the primary velocity, Local and average shear stress in *x*-axis of the flow.

porosity parameter is enhance then the primary velocity, shear stress profiles are increased. Because when porosity parameter is increased then porous layer is extended, So primary velocity increases.

Figures 12 (a, b, c) displayed that the primary velocity, Local and average shear stress in x-axis decrease with increase of magnetic parameter M. When magnetic parameter is increased then created a drag force such as Lorentz force which serves to retard the primary fluid velocity. Whereas secondary velocity, local and average shear stress in z–axis have reverse effect with the increasing values of magnetic parameter which are displayed in Figures 13 (a, b, c). This is because that the resulting Lorentzian body force will not perform as a drag force as in conventional MHD flows, but as an aiding body force. So the secondary fluid velocity, local and average shear stress in z–axis are increased.

It is clear that form Figure 14 (a), the temperature distribution increases with the increasing value of magnetic parameter. The transverse magnetic field to an electrically conducting fluid gives rise a drag force which is called the Lorentz force. Hence Lorentz force increases temperature profiles. But Local and average Nusselt numbers has decreasing effect which are shown in Figures 14 (b, c).

Figures 15 (a, b, c) demonstrate that the primary velocity (U), local and average shear stresses in x-axis decrease with increases of Prandtl number P_r. It is noted from Figure 16 (a), temperature $(\bar{T})$ distributions decreases with the increase of Prandtl number. On the otherhand the local and average Nusselt numbers (N_{uL}, N_{uA}) have opposite behavior have been illustrate with the increases of Prandtl number is displayed in Figure 16 (b, c).

From Figure 17 (a, b, c) it is found that the primary velocity (U), local and average shear stresses in x-axis (τ_{LU}, τ_{AU}) profiles increase with an increase of Soret number(S_0). Figure 18 (a) displayed that the concentration $(\bar{C})$ distribution enhance with the increase of Soret number. Because when the Soret number is increased, the concentration boundary layer thickness increases. The local and average Sherwood numbers (S_{hL}, S_{hA}) are reduced with the increasing values of Soret number which are illustrated in Figure 18 (b, c).

It is seen from Figure 19 (a), primary velocity profiles decreases firstly, then start to increase with increase of rotational parameter (R). So there is a cross flow near $Y = 20.0$ (approximately). This due to the fact that rotation retards primary flow in the boundary layer. But local and average shear stresses in x-axis have reverse effect which are shown in Figure 19 (b, c).

In Figure 20 (a), it has been illustrated that primary velocity (U) decreases firstly, then start to increase with increase of inertia parameter (Γ). So there is cross flow near $Y = 11.0$ (approximately). The medium inertia (Γ) effects constitute resistance to flow. The resistance to the flow increases when inertia parameter (Γ) increases, causing the fluid flow to slow down. The local and average shear stresses in x-axis (τ_{LU}, τ_{AU}) are decreased with the increase of inertia parameter which is displayed by Figure 20 (b, c).

From Figure 21 (a) it is seen that, firstly the primary velocity (U) decreases up to $Y = 20.0$ but after that (U) increases with increases of permeability parameter (γ). Because for increasing values of permeability parameter the resistance of the porous medium is raised. The local and average shear stresses in x-axis (τ_{LU}, τ_{AU}) are decreased which are seen in Figure 21 (b, c).

Finally, a comparison of the present results with the published results of [31] is presented in table 1. The present results is good in case of flow parameters.

Figure-5(a). Primary velocity profiles for different values of β_e.

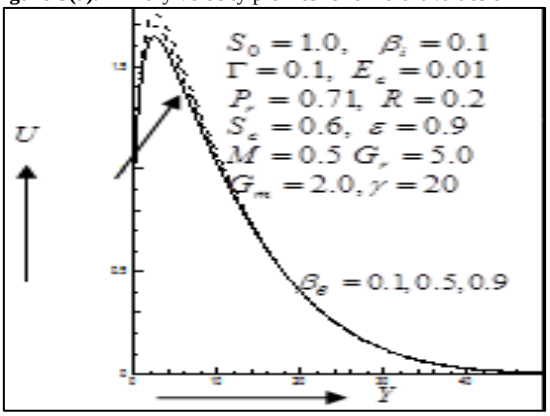

Figure-5(b). Local shear stress in X -direction for different values of β_e

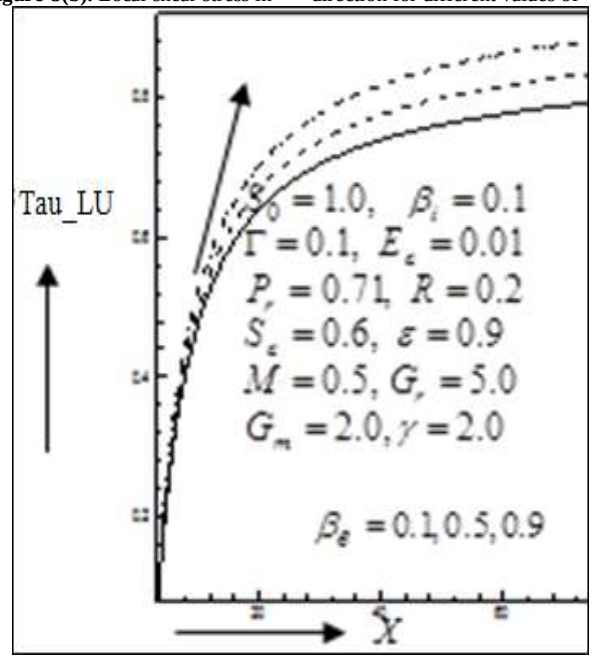

Figure-5(c). Average Shear stress in X - axis for different values of β_e

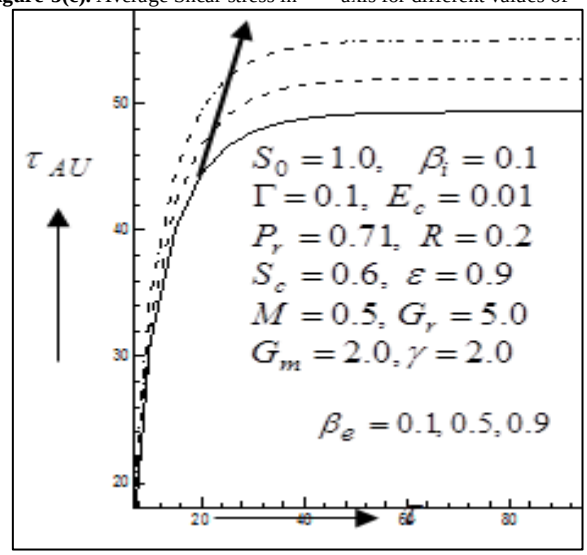

Figure-6(a). Temperature profiles for different values of β_e

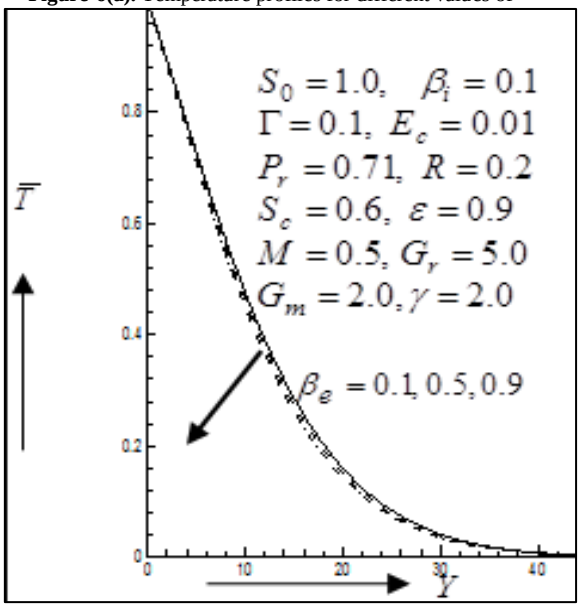

Figure-6(b). Local Nusselt number for different values of β_e

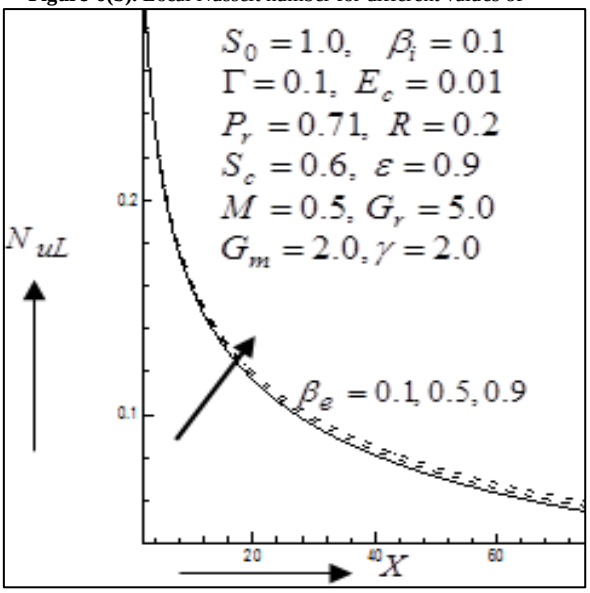

Figure-6(c). Average Nusselt number for different values of β_e

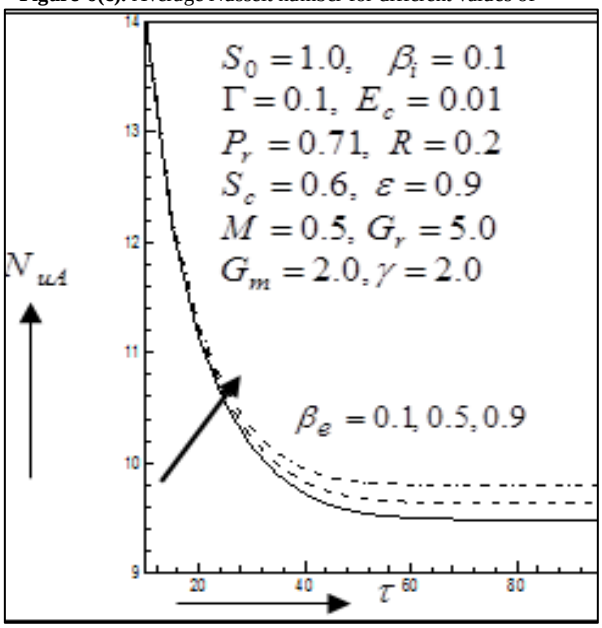

Figure-7(a). Primary velocity profiles for different values of β_i

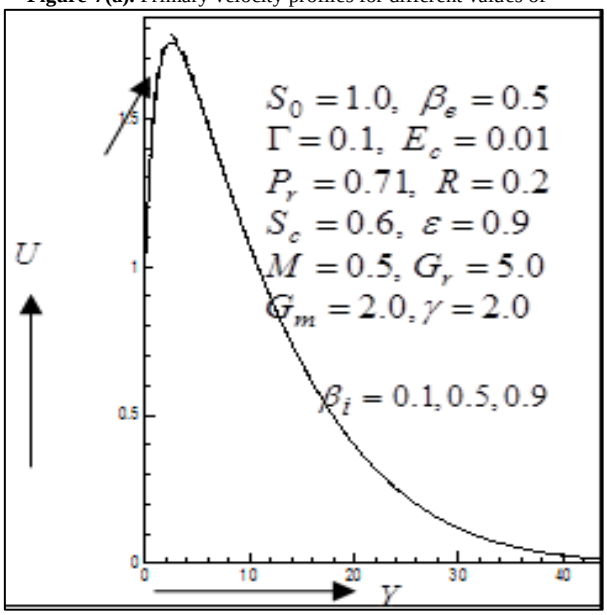

Figure-7(b). Local Shear stress in x -direction for different values of β_i

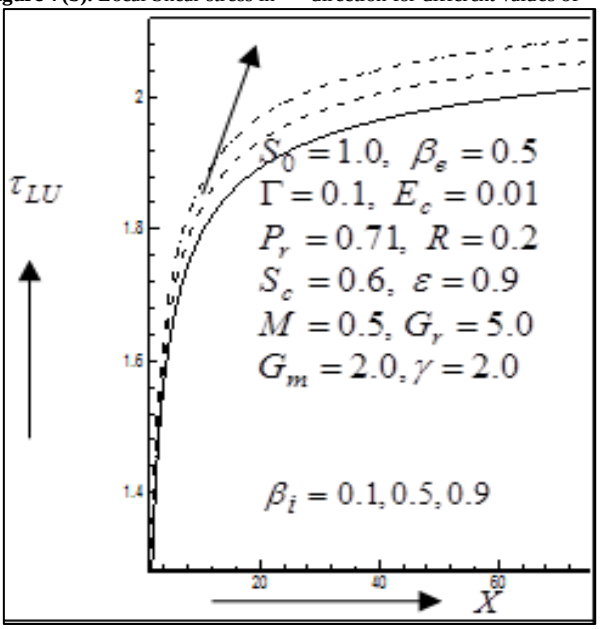

Figure-7(c). Average Shear stress in x -axis for different values of β_i

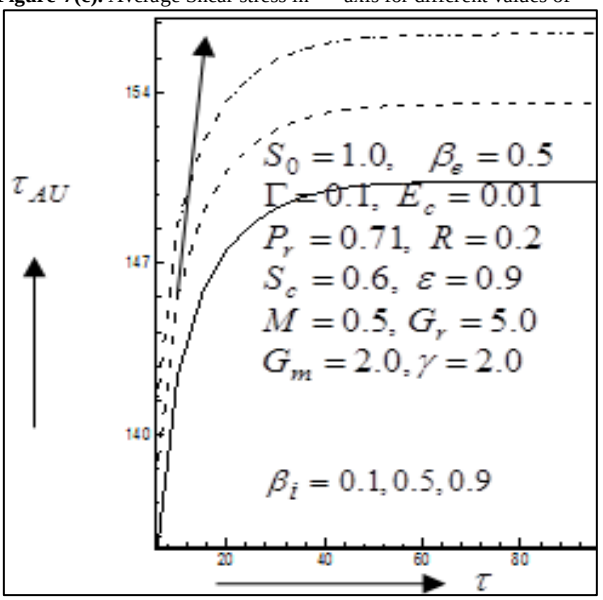

Figure-8(a). Secondary velocity profiles for different values of β_i

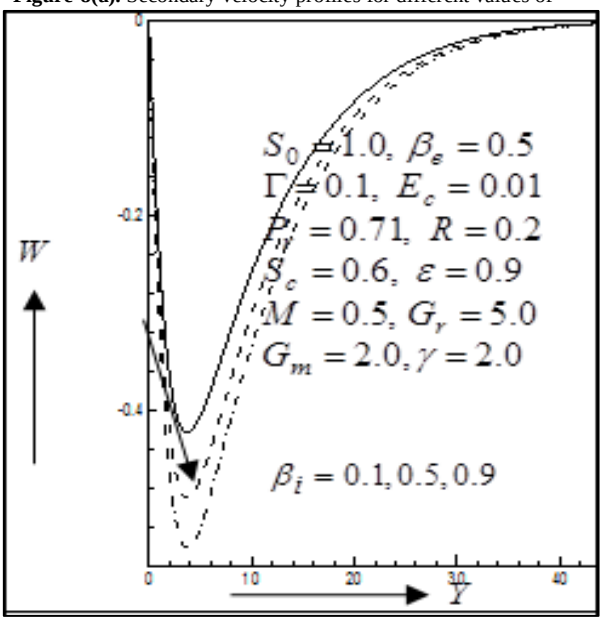

Figure-8(b). Local Shear stress in z -axis for different values of β_i

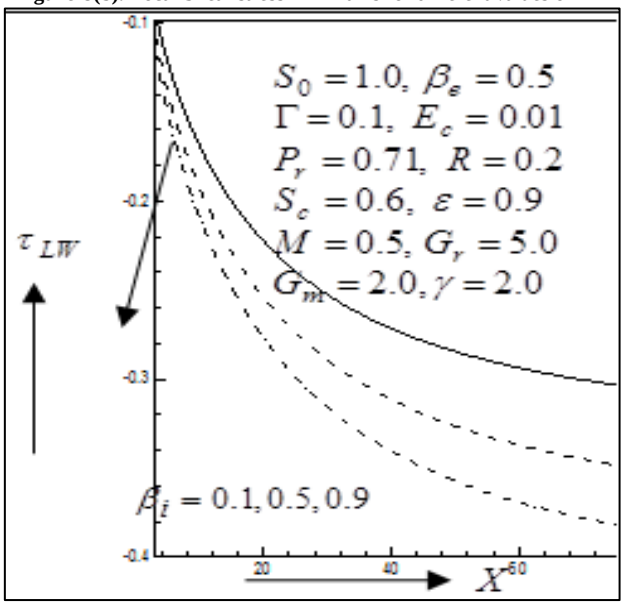

Figure-8(c). Average Shear stress in z -axis for different values of β_i

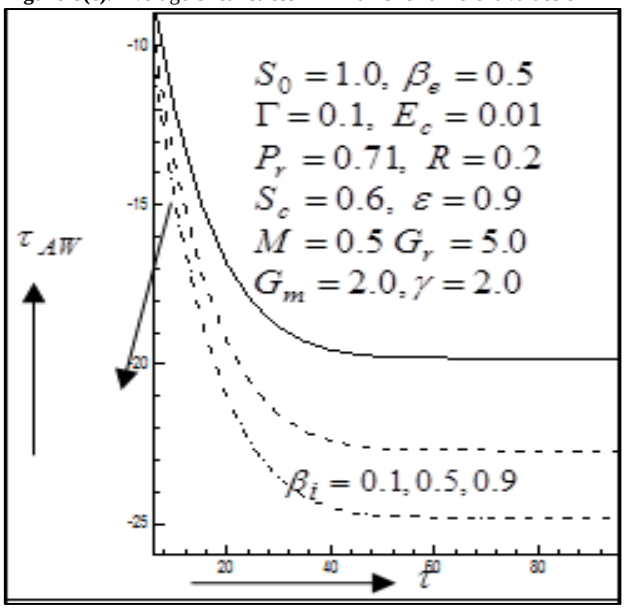

Figure-9(a). Primary velocity profiles for different values of E_c

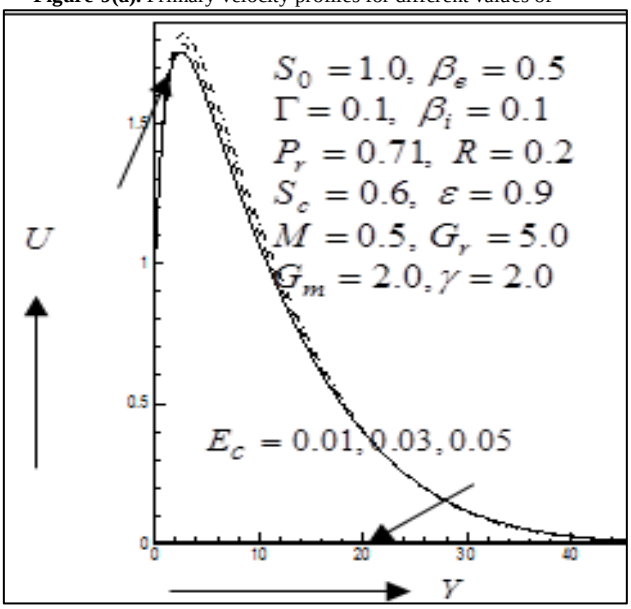

Figure-9(b). Local Shear stress in x - direction for different values of E_c

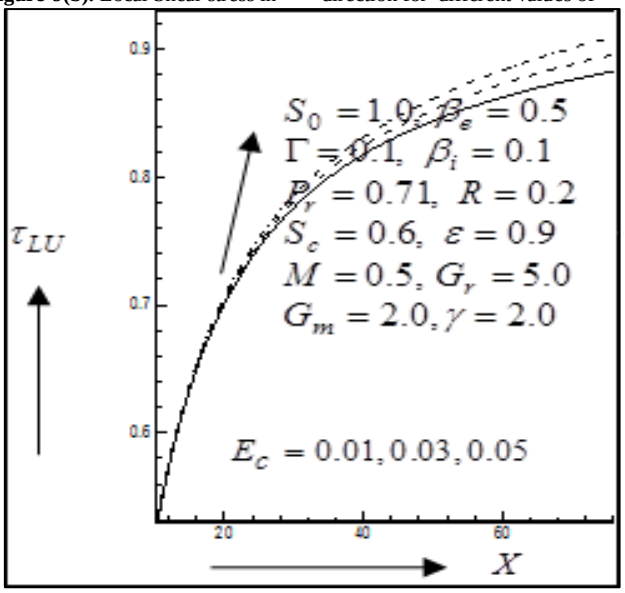

Figure-9(c). Average Shear stress in x -axis for different values of E_c

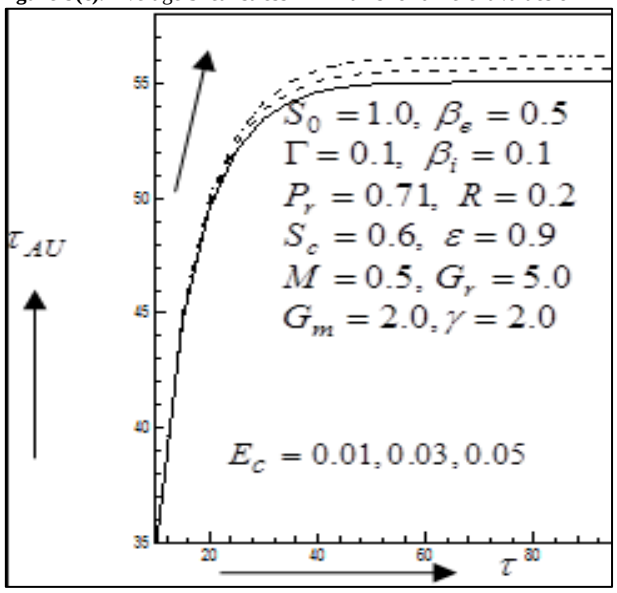

Figure-10(a). Temperature profiles for different values of E_c

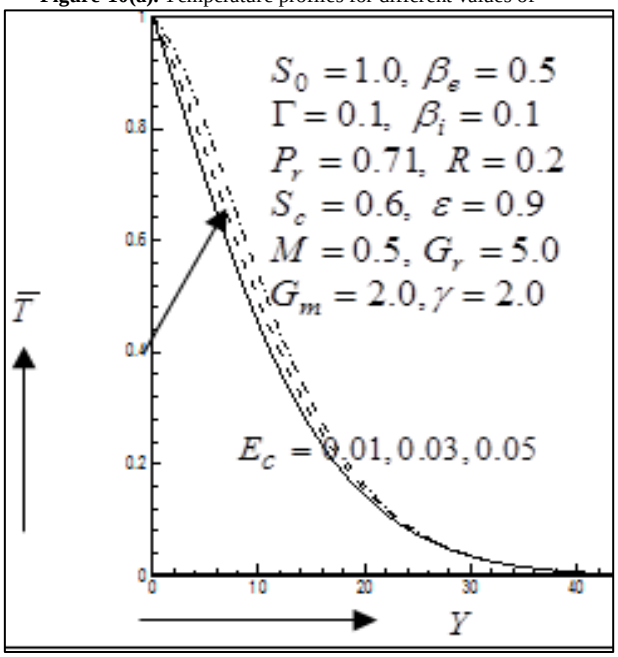

Figure-10(b). Local Nusselt number for different values of E_C

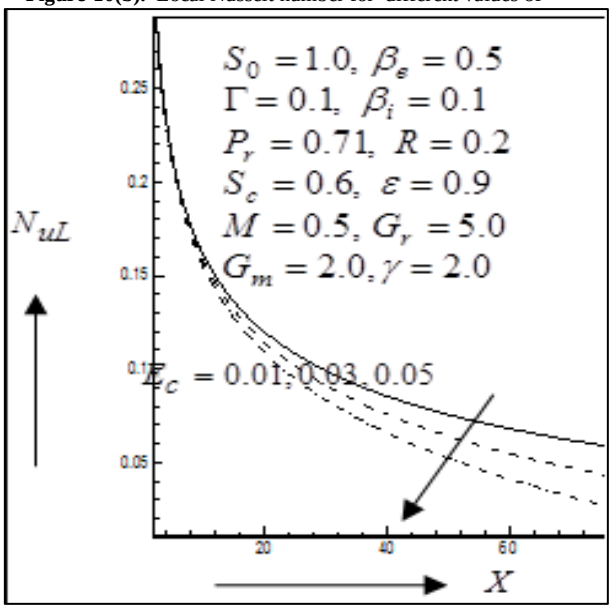

Figure-10(c). Average Nusselt number for different values of E_c

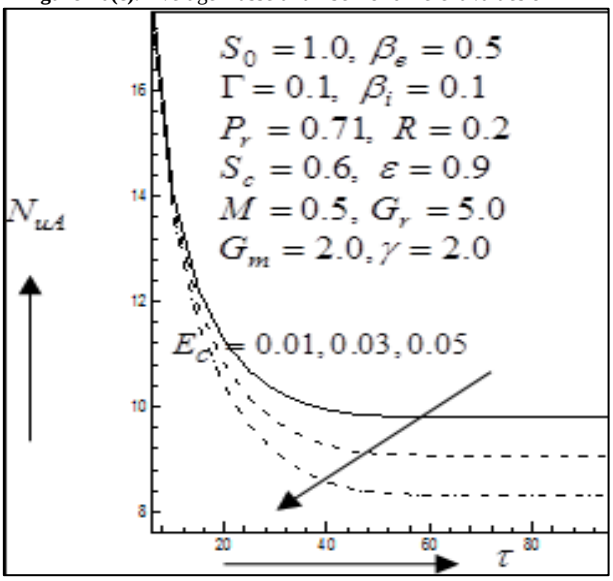

Figure-11(a). Primary velocity profiles for different values of ε

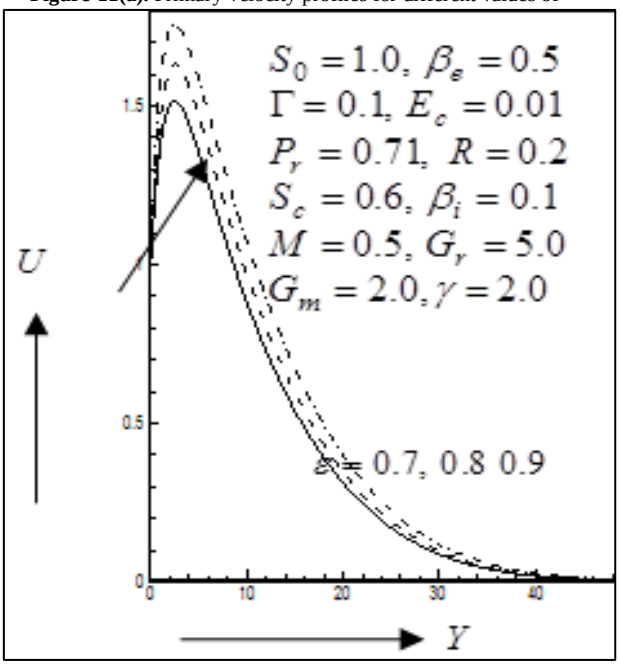

Figure-11(b). Local Shear stress in X -direction for different values of ε

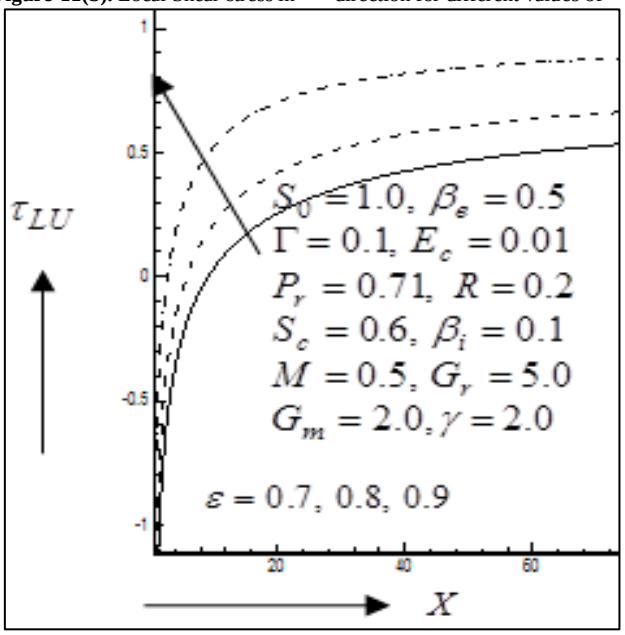

Figure-11(c). Average Shear stress in X -axis for different values of ε

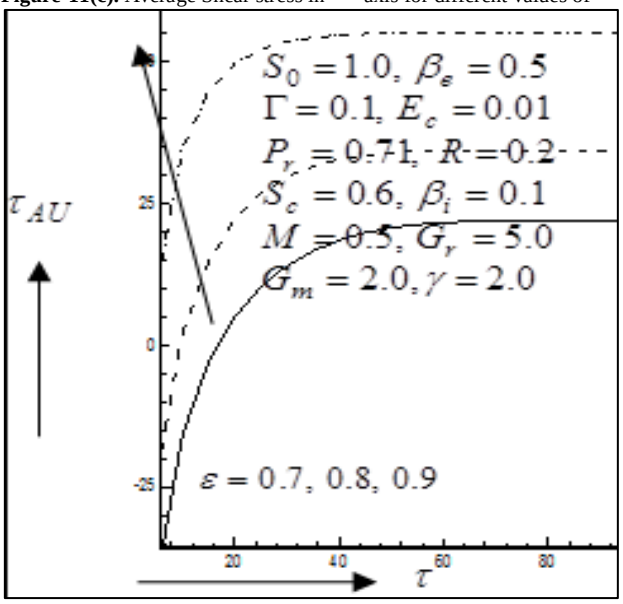

Figure-12(a). Primary velocity profiles for different values of M

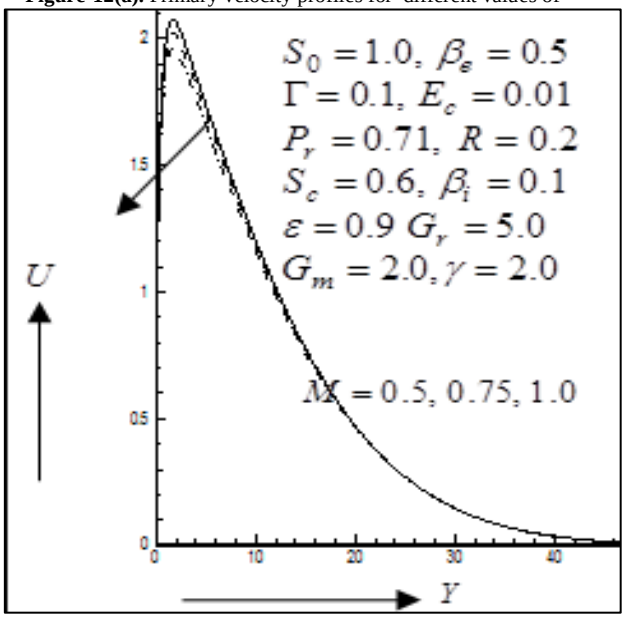

Figure-12(b). Local Shear stress in x -direction for different values of M

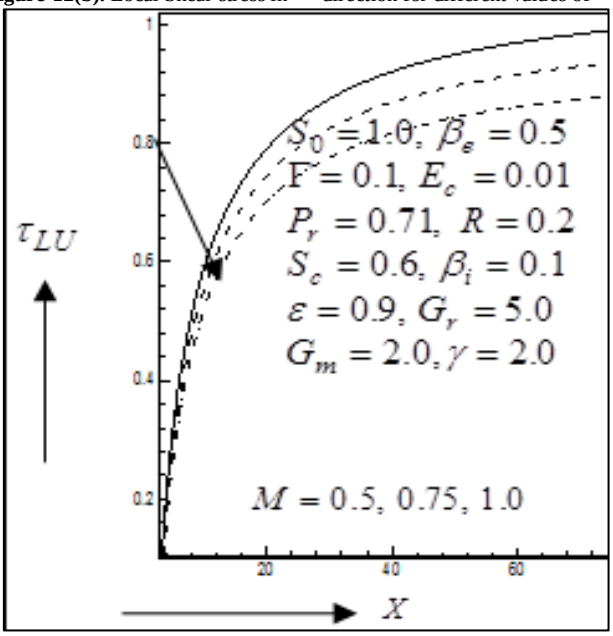

Figure-12(c). Average Shear stress in x -axis for different values of M

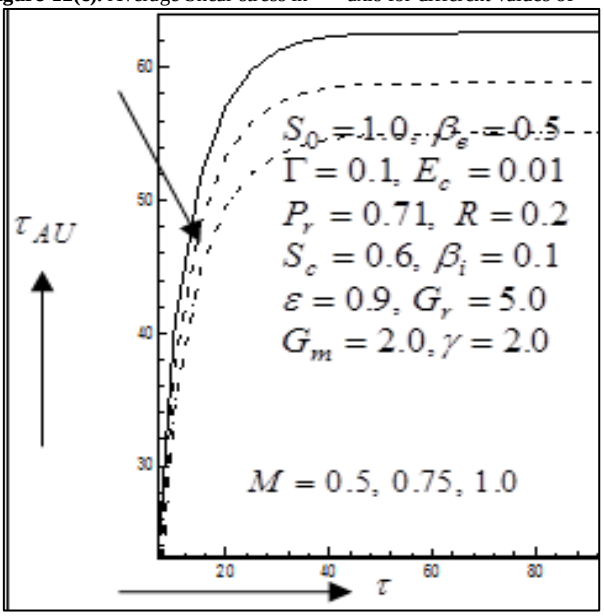

Figure-13(a). Secondary velocity profiles for different values of M

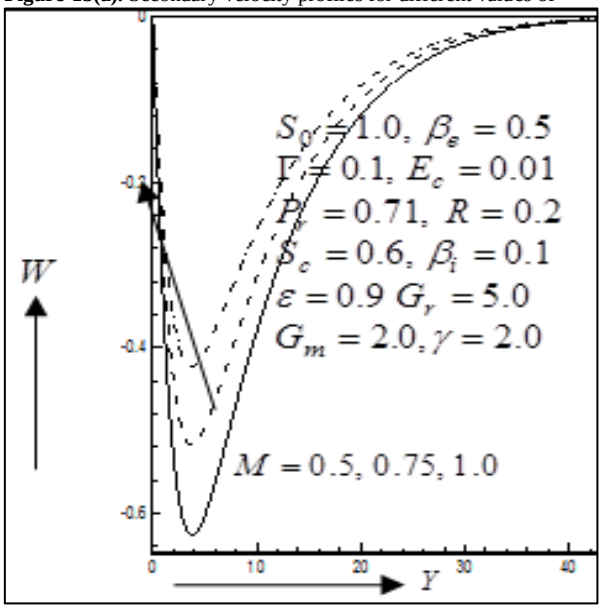

Figure-13(b). Local Shear stress in Z -axis for different values of M

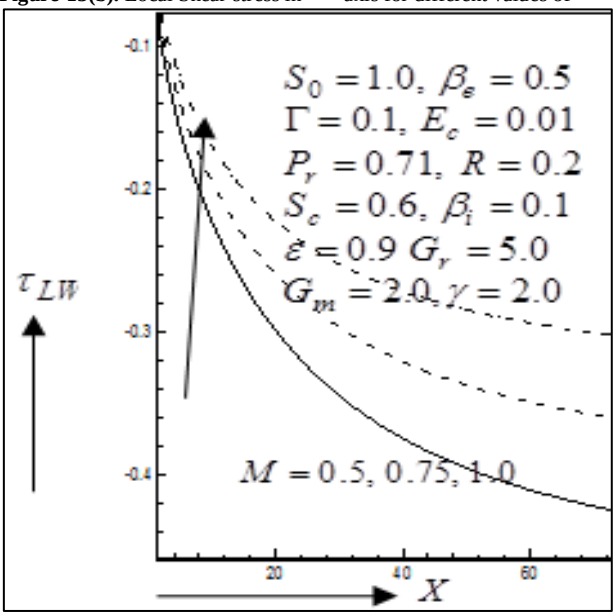

Figure-13(c). Average Shear stress in Z -axis for different values of M

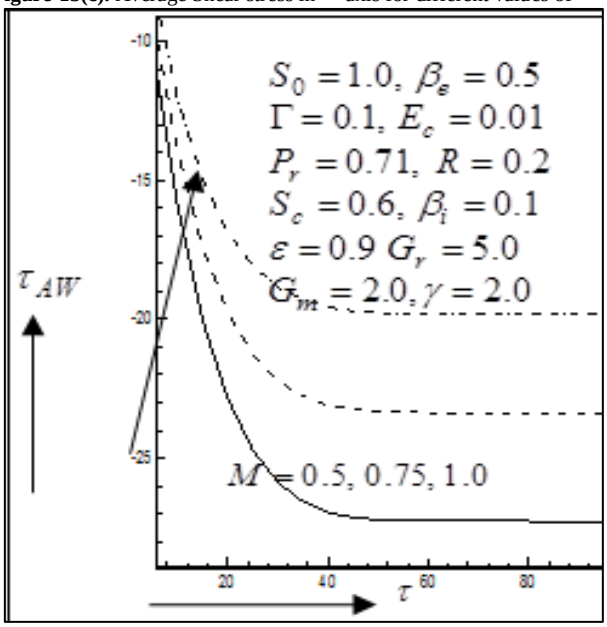

Figure-14(a). Temperature profiles for different values of M

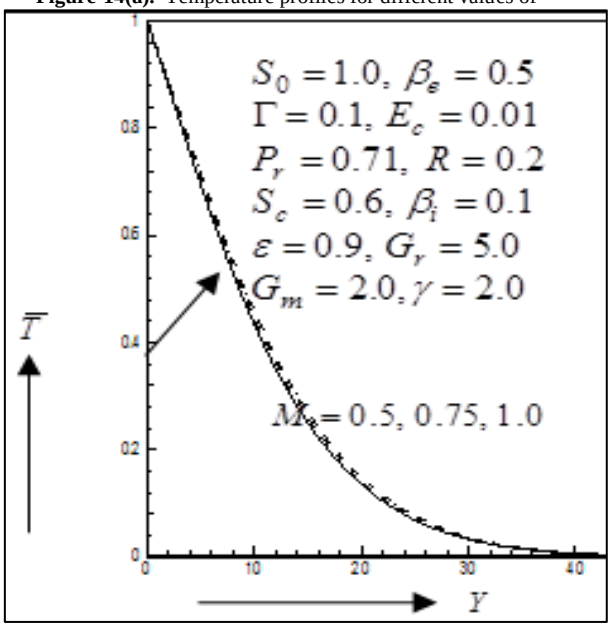

Figure-14(b). Local Nusselt number for different values of M

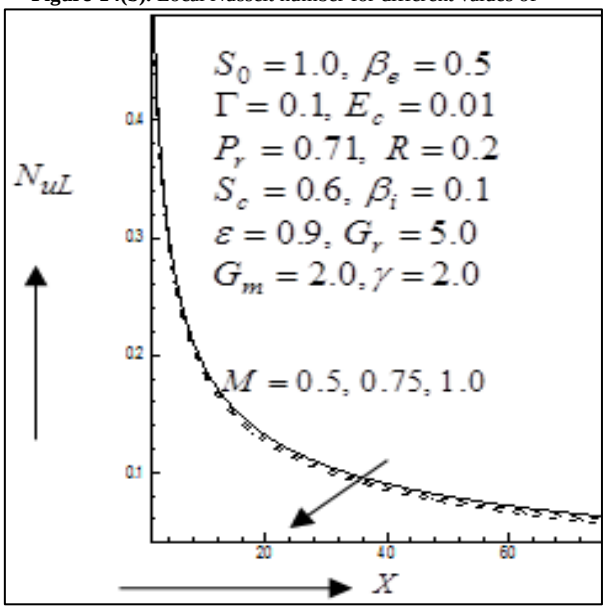

Figure-14(c). Average Nusselt number for different values of M

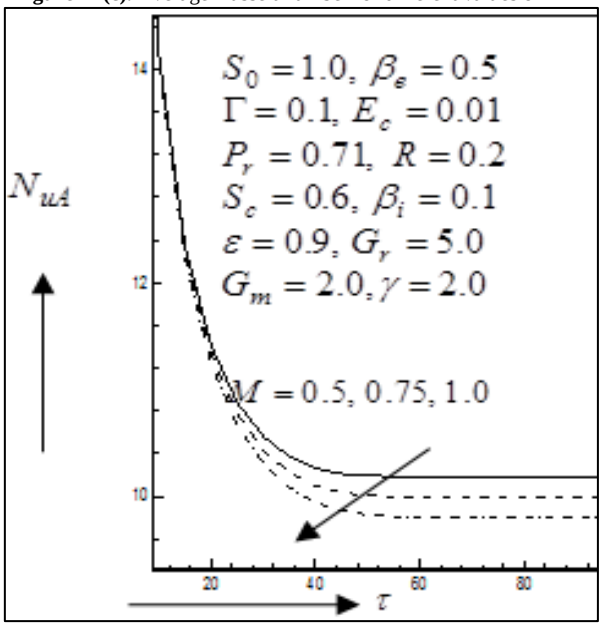

Figure-15(a). Primary velocity profiles for different values of P_r

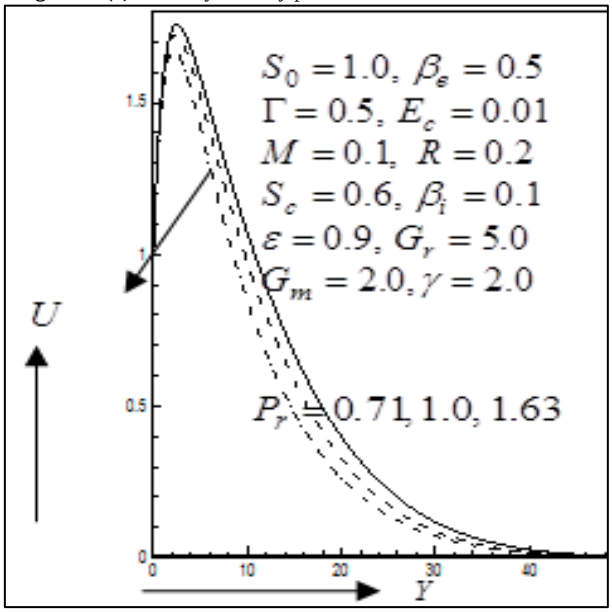

Figure-15(b). Local Shear stress in x -axis for different values of P_r

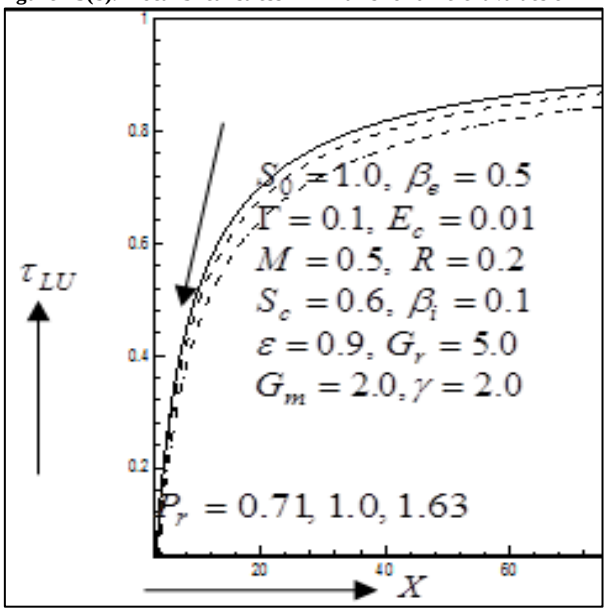

Figure-15(c). Average Shear stress in x -axis for different values o P_r

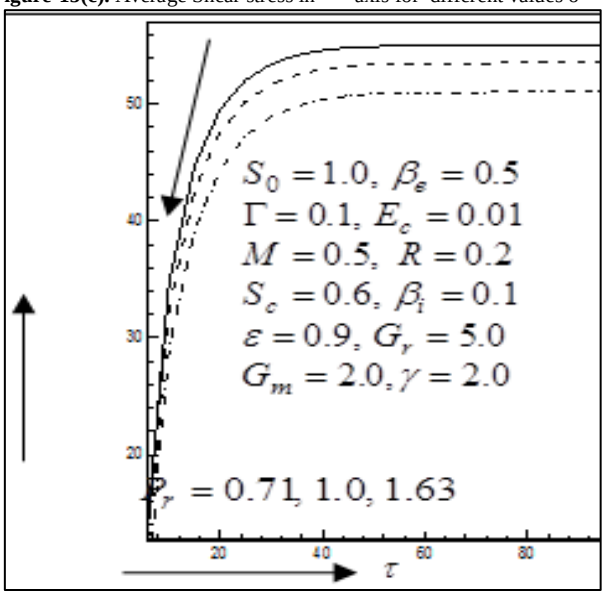

Figure-16(a). Temperature profiles for different values of P_r

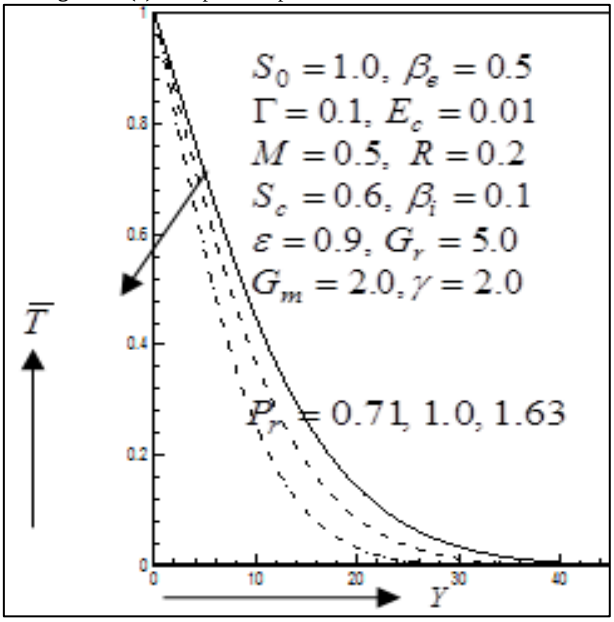

Figure-16(b). Local Nusselt number for different values of P_r

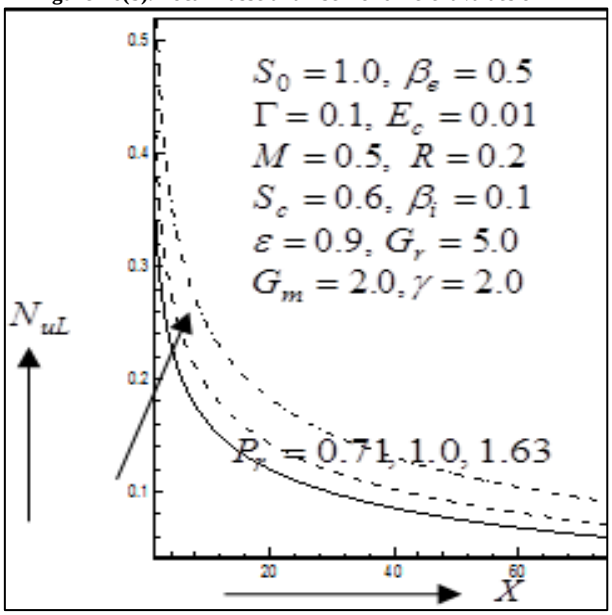

Figure-16(c). Average Nusselt number for different values of P_r

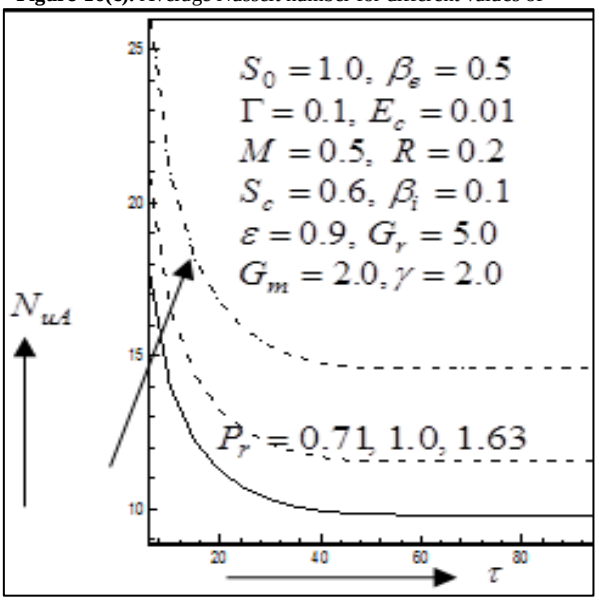

Figure-17(a). Primary velocity profiles for different values of S_0

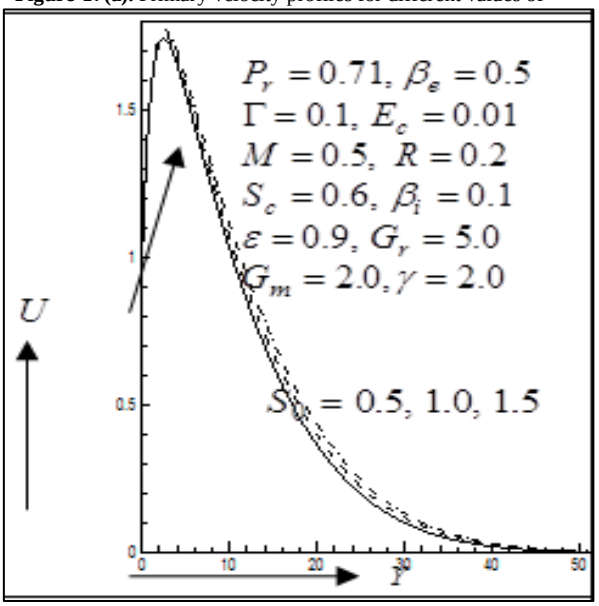

Figure-17(b). Local Shear stress in X - axis for different values of S_0

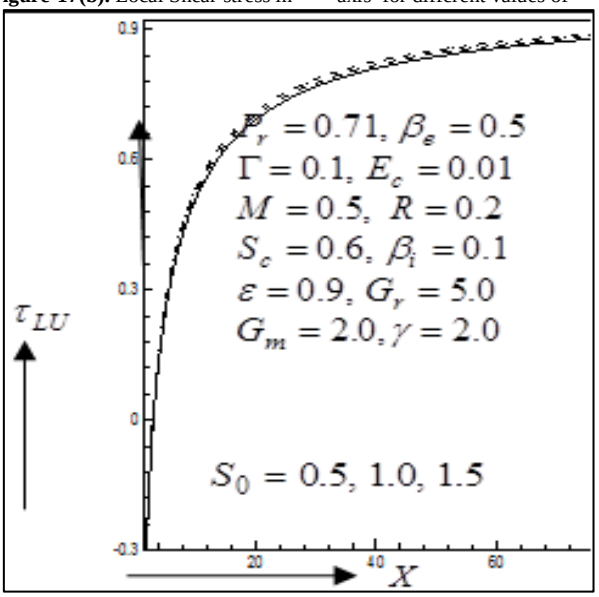

Figure-17(c). Average Shear stress in X - axis for different values of S_0

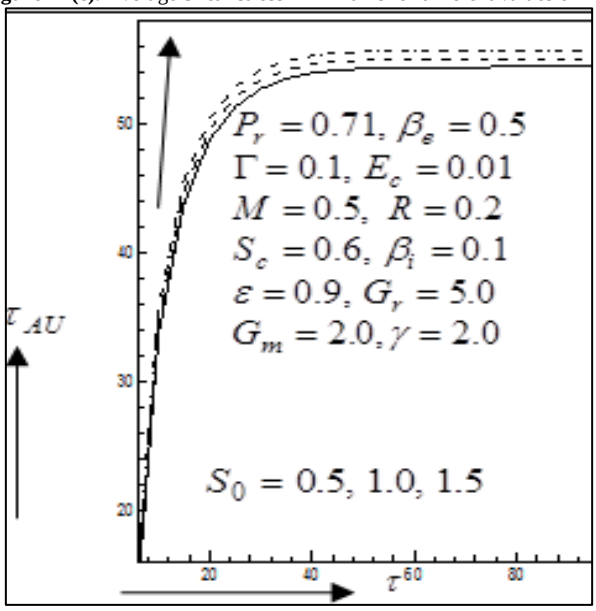

Figure-18(a). Concentration profiles for different values of S_0

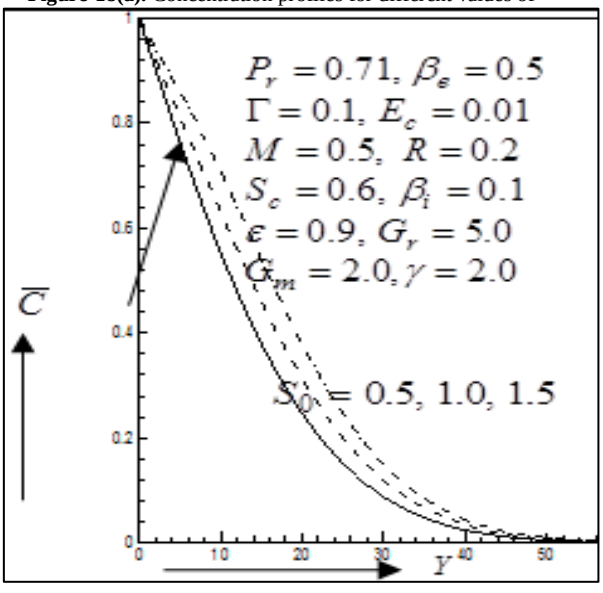

Figure-18(b). Local Sherwood number for different values of S_0

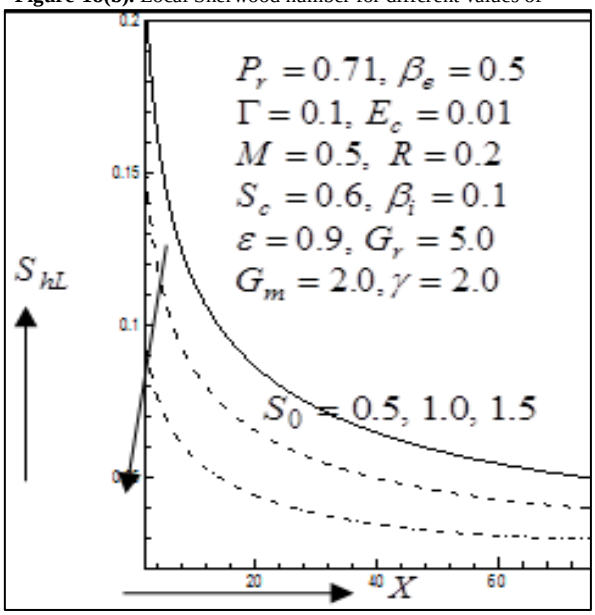

Figure-18(c). Average Sherwood number for different values of S_0

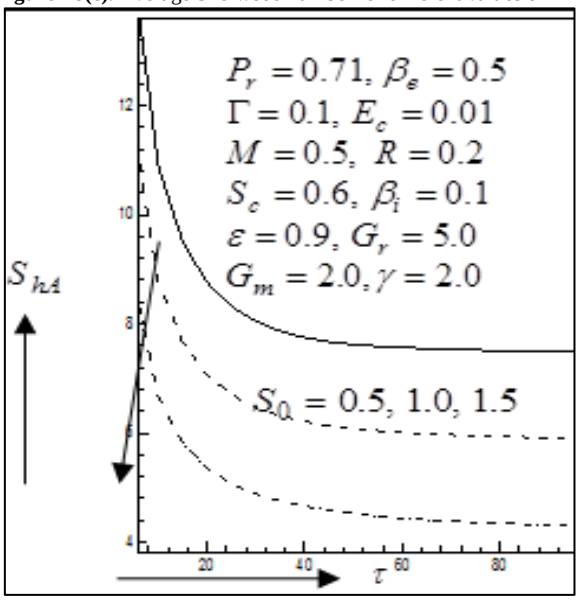

Figure-19(a). Primary velocity profiles for different values of R

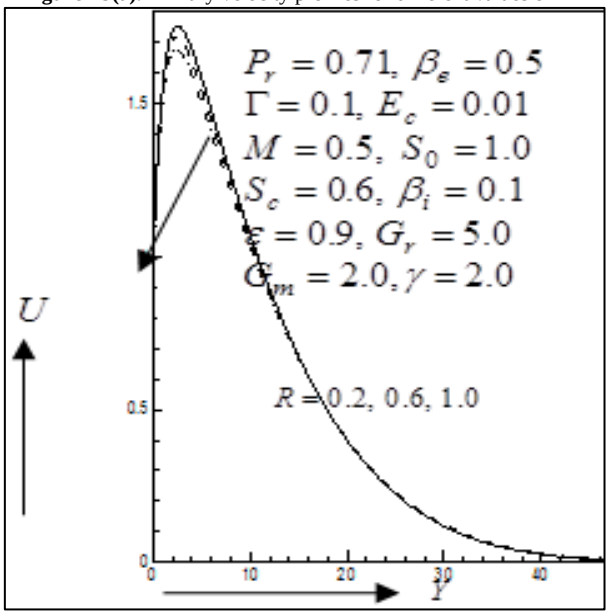

Figure19(b). Local Shear stress in X -axis for different values of R

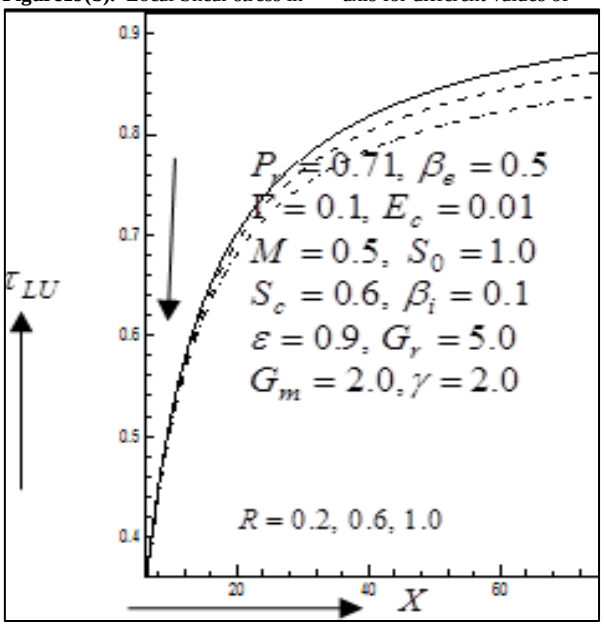

Figure-19(c). Average Shear stress in X -axis for different values of R

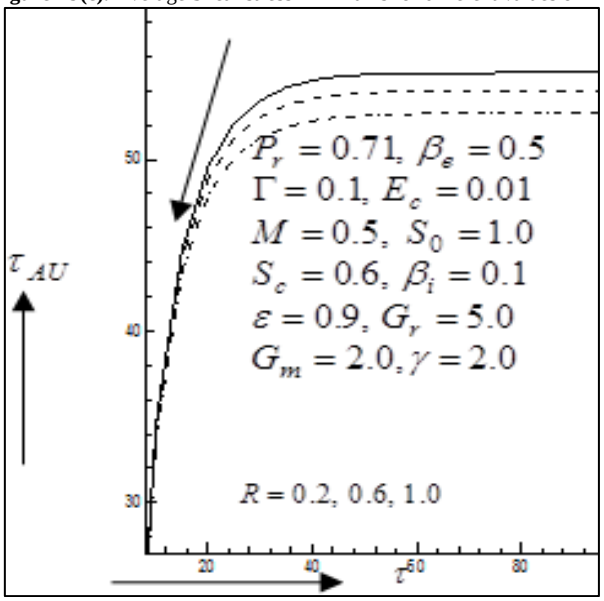

Figure-20(a). Primary velocity profiles for different values of Γ

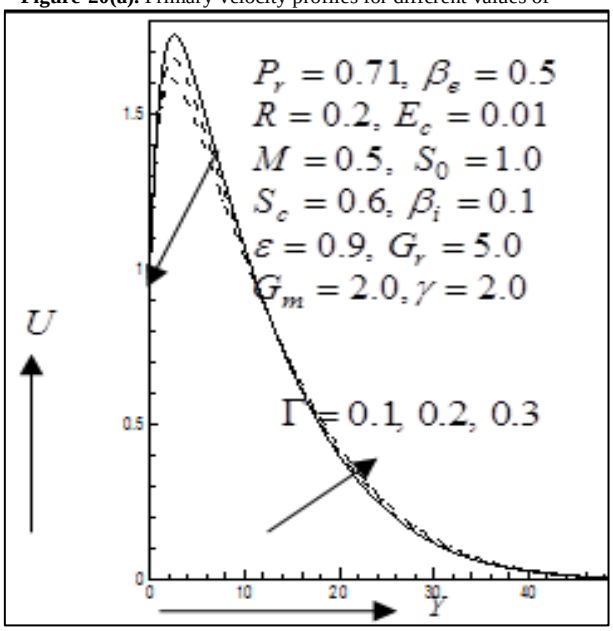

Figure-20(b). Local Shear stress in X -axis for different values of Γ

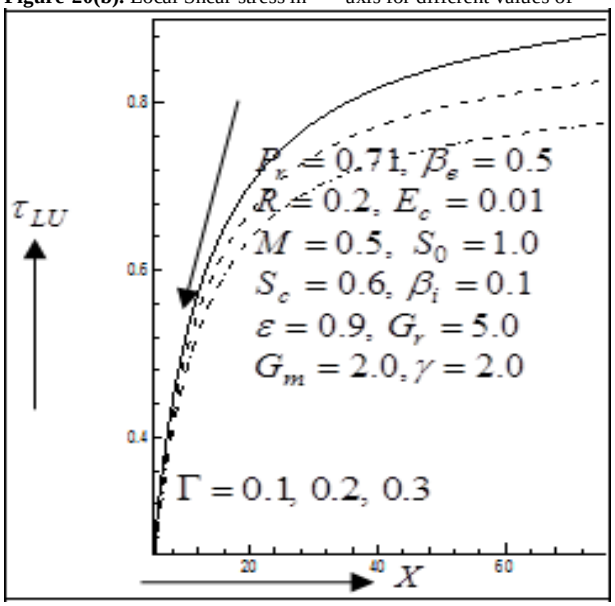

Figure-20(c). Average Shear stress in X -axis for different values of Γ

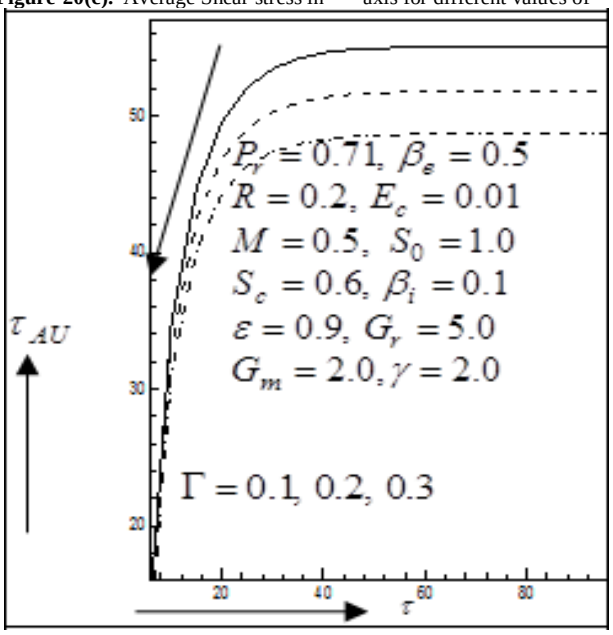

Figure-21(a). Primary velocity profiles for different values of γ

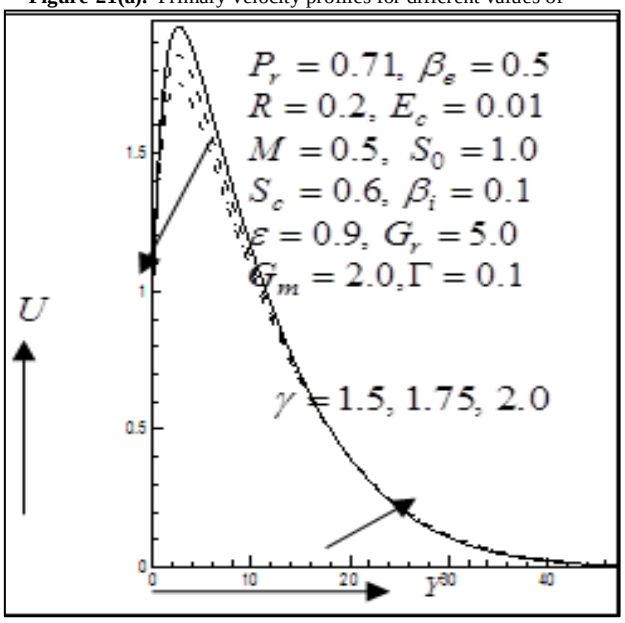

Figure-21(b). Local Shear stress in X -axis for different values of γ

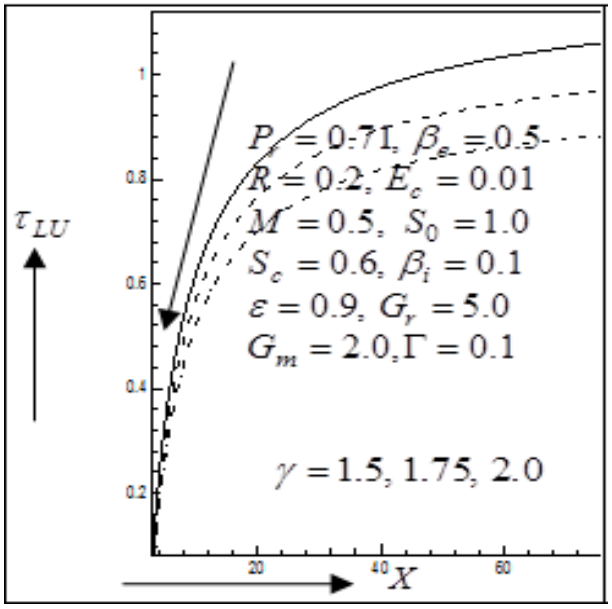

Figure-21(c). Average Shear stress in X -axis for different values of γ

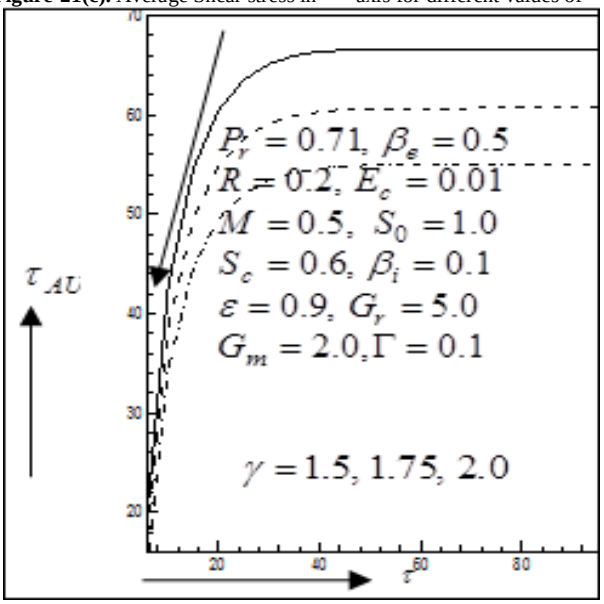

6. Comparison

Table-1. A comparison of the present results with the previous results

Increased Parameters	**Pervious Published results of Mahmud, *et al.* [31]**				**Present results**			
	$\frac{u}{U_0}$	g_0	θ	ϕ	U	W	$\bar{T}$	$\bar{C}$
M	Dec	Inc	-	-	Dec	Inc	Inc	-
E_c	Inc	-	-	-	Inc	-	Inc	-
P_r	Dec	-	Dec	-	Dec	-	Dec	-
S_0	Inc	-	-	Inc	Inc	-	-	Inc
R	Dec	-	-	-	Dec	-	-	-

7. Conclusions

An unsteady Hall and ion-slip currents effects on heat and mass transfer flow in a revolving system with high porosity medium in presence of magnetic field have been solved numerically by finite difference method with the associated boundary conditions. The numerical outcomes of the present article are presented graphically. The outcome of the numerical results are given below:

a) The primary velocity, local and average shear stresses in X-axis in the flow direction are increased with enhance of Hall and ion-slip parameter, Eckert number, porosity parameter and Soret number whereas those are decreased with enhance of magnetic parameter, Prandtl number, rotation parameter, inertia parameter, permeability parameter.
b) The secondary velocity, the local and average shear stresses in Z-axis are raised with the increasing values of magnetic parameter while those are reduced with enhance of ion-slip parameter.
c) The temperature distributions are raised with the increase of Eckert number, magnetic parameter whereas it reduces with enhance of Hall parameter, Prandtl number.
d) Local and average Nusselt numbers are enhanced with the increase of Hall parameter, Prandtl number but those are reduced with enhance of Eckert number, magnetic parameter.
e) It is clearly revealed that the effect of Soret number is to enhance the concentration profiles in the flow region whereas a reverse pattern have been shown in local and average Sherwood numbers with enhance of Soret number.

References

[1] Cowling, T. G., 1933. "The magnetic field of sunspots." *Monthly Notices of the Royal Astronomical Society*, vol. 94, pp. 39-48.
[2] Ferraro, V. C. A., 1937. "The non-uniform rotation of the sun and its magnetic field." *Monthly Notices of the Royal Astronomical Society*, vol. 97, pp. 458-472.
[3] Hartmann, J., 1937. "Flow in pipes under transverse magnetic field." *Matematisk-Fysiske Meddelelser*, vol. 15, pp. 6-7.
[4] Gebhart, B., 1962. "Effects of viscous dissipation in natural convection." *Journal of Fluid Mechanics*, vol. 14, pp. 225–232.
[5] Schwartz, C. E. and Smith, J. M., 1953. "Flow distribution in packed beds." *Industrial and Engineering Cheministry*, vol. 45, pp. 1209-1218.
[6] Vafai, K. and Tien, C. L., 1981. "Boundary and inertia effects on flow and heat transfer in porous media." *International Journal of Heat and Mass Transfer*, vol. 24, pp. 195-203.
[7] Chen, C. K. and Lin, C. R., 1995. "Natural convection from an isothermal vertical surface embedded in a thermally stratified high-porosity medium." *International Journal of Engineering Science*, vol. 33, pp. 131-138.
[8] Chamkha, A. J., Harmindar, S., and Takhar, G. N., 2005. "Natural convection flow in a rotating fluid over a vertical plate embedded in a thermally stratified high-porosity medium." *International Journal of Fluid Mechanics Research*, vol. 32, pp. 511-527.
[9] Foisal, A. A. and Alam, M. M., 2016. "Unsteady free convection fluid flow over an inclined plate in the presence of a magnetic field with thermally stratified high porosity medium." *Journal of Applied Fluid Mechanics*, vol. 9, pp. 1467-1475.
[10] Anwar, B. O., Takhar, H. S., Tasveer, A. B., Chamkha, A. J., and Girishwar, N. R. M., 2005. "Modelling convection heat transfer in a rotating fluid in a thermally-stratified high-porosity medium: numerical finite difference solutions." *International Journal of Fluid Mechanics Research*, vol. 32, pp. 383-401.
[11] Venkata, M. J., Raja, S. M. N., and Shashidar, R. B., 2017. "Unsteady MHD free convection flow past a semi-infinite moving vertical plate with Soret and Dufour effects." *Current Trends in Technology and Science*, vol. 6, pp. 715-719.
[12] Bhuvanavijaya, R. and Mallikarjuna, B., 2014. "Effect of variable thermal conductivity on convective heat and mass transfer over a vertical plate in a rotating system with variable porosity regime." *Journal of Naval Architecture and Marine Engineering*, vol. 11, pp. 83-92.
[13] Chen, C. K., Hung, C. I., and Horng, W. C., 1987. "Transient natural convection on a vertical flat plate embedded in a high-porosity medium." *Journal of Energy Resources Technology*, vol. 109, pp. 112-118.
[14] Suneetha, K., Mohammed, I. S., and Ramana, R. G. V., 2019. "A study on free convective heat and mass transfer flow through a highly porous medium with radiation, chemical reaction and Soret effects." *Journal of Computational and Applied Research in Mechanical Engineering*, vol. 8, pp. 121-132.
[15] Reddy, P. B., 2016. "Mass transfer effects on an unsteady MHD free convective flow of an incompressible viscous dissipative fluid past an infinite vertical porous plate." *International Journal of Applied Mechanics and Engineering*, vol. 21, pp. 143-155.
[16] Dash, K., Alam, M. M., and Wahiduzzaman, M., 2012. "MHD free convection and mass transfer flow from a vertical plate in the presence of Hall and ion-slip current." *Advances in Mechanical Engineering*, pp. 1-20. Available: https://journals.sagepub.com/doi/10.1155/2012/851957
[17] Naroua, H., 2007. "A computational solution of hydromagnetic free convective flow past a vertical plate in a rotating heat-generating fluid with Hall and ion-slip currents." *International Journal for Numerical Methods in Fluids*, vol. 53, pp. 1647-1658.
[18] Mahendar, D. and Rao, S. P., 2015. "The effect of Hall current on an unsteady MHD free convective flow along a vertical porous plate with thermal radiation." *IOSR Journal of Mathematics*, vol. 11, pp. 122-141.
[19] Abuga, J. G., Kinyanjui, M., and Sigey, J. K., 2011. "An investigation of the effect of Hall current and rotational parameter on dissipative fluid flow past a vertical semi-infinite plate." *Journal of Engineering and Technology Research*, vol. 3, pp. 314-320.

[20] Seth, G. S., Kumbhakar, B., and Sharma, R., 2015. "Unsteady hydromagnetic natural convection flow of a heat absorbing fluid within a rotating vertical channel in porous medium with Hall effects." *Journal of Applied Fluid Mechanics*, vol. 8, pp. 767-779.

[21] Ferdows, M., Jahan, E., Hamad, M. M., and Masahiro, O., 2011. "Effects of Hall and ion- slip currents on free convective heat transfer flow past a vertical plate considering slip conditions." *Canadian Journal on Science and Engineering Mathematics*, vol. 2, pp. 70-76.

[22] Krishna, M., Veera, Swarnalathamma, B. V., and Chamkha, A. J., 2019. "Investigations of Soret, Joule and Hall effects on MHD rotating mixed convective flow past an infinite vertical porous plate." *Journal of Ocean Engineering and Science*, vol. 4, pp. 263–275.

[23] Veera, Krishna, M., Ameer, A. N., and Chamkha, A. J., 2020. "Hall and ion slip effects on unsteady MHD free convective rotating flow through a saturated porous medium over an exponential accelerated plate." *Alexandria Engineering Journal*, vol. 59, pp. 565-577.

[24] Sarma, D. and Pandit, K. K., 2018. "Effects of Hall current, rotation and Soret effects on MHD free convection heat and mass transfer flow past an accelerated vertical plate through a porous medium." *Ain Shams Engineering Journal*, vol. 9, pp. 631-646.

[25] Jitendra, K. S. and Srinivasa, C. T., 2018. "Unsteady natural convection flow of a rotating fluid past an exponential accelerated vertical plate with Hall current, ion-slip and magnetic effect." *Multidiscipline Modeling in Materials and Structures*, vol. 14, pp. 216–235.

[26] Srinivasa, R. G., Ramana, B., Rami, R. B., and Vidyasagar, G., 2014. "Soret and Dufour effects on MHD boundary layer flow over a moving vertical porous plate with suction." *International Journal of Emerging Trends in Engineering and Development*, vol. 2, pp. 215-226.

[27] Rajput, U. S. and Mohammad, S., 2017. "Unsteady MHD convective flow along vertical exponentially accelerated flat plate with variable temperature through porous medium in the presence of Hall current, in a rotating system." *International Journal for Research in Applied Science and Engineering Technology*, vol. 5, pp. 793-800.

[28] EL-Kabeir, S. M., Modather, M., and Rashad, A. M., 2015. "Heat and mass transfer by unsteady natural convection over a moving vertical plate embedded in a saturated porous medium with chemical reaction, Soret and Dufour effects." *Journal of Applied Fluid Mechanics*, vol. 8, pp. 453-463.

[29] Ahmed, N. and Goswami, J. K., 2011. "Hall effect on MHD forced convection from an infinite porous plate with dissipative heat in a rotating system." *Turkish Journal of Physics*, vol. 35, pp. 293-302.

[30] Chandra, S. K. V., 2018. "MHD free convective heat and mass transfer flow past an accelerated vertical plate through a porous medium with Hall current, rotation and Soret effects." *International Journal of Mechanical and Production Engineering Research and Development*, vol. 8, pp. 685-706.

[31] Mahmud, A. M., Delowar, H. M., and Arif, H. M., 2011. "Viscous dissipation and Joule heating effects on steady MHD combined heat and mass transfer flow through a porous medium in a rotating system." *Journal of Naval Architecture and Marine Engineering*, vol. 2, pp. 105-120.

[32] Prasanna, L. M., Bhaskar, R. N., and Poornima, T., 2012. "MHD boundary layer flow of heat and mass transfer over a moving vertical plate in a porous medium with suction and viscous dissipation." *International Journal of Engineering Research and Applications*, vol. 2, pp. 149-159.

[33] Siva, R. S. and Srinivasa, R. R., 2016. "Transient MHD free convective flow past an infinite vertical plate embedded in a porous medium with viscous dissipation." *Meccanica*, vol. 51, pp. 1057-1068.